Contents lists available at ScienceDirect

Optics & Laser Technology
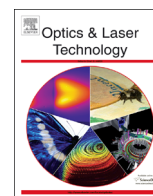
Effect of laser pulse energy and wavelength on the structure, morphology and optical properties of ZnO nanoparticles

Elmira Solati, Laya Dejam, Davoud Dorranian *

Laser Lab., Plasma Physics Research Center, Science and Research Branch, Islamic Azad University, Tehran, Iran

ARTICLE INFO

ABSTRACT

In this work, the effects of the laser pulse energy and laser wavelength on the production of ZnO nanoparticles prepared by pulsed laser ablation of Zn metal plate in deionized water are investigated. The beam of a Q-switched Nd:YAG laser of 1064 and 532 nm wavelengths at 6 ns pulse width and different fluences is employed to irradiate the solid target in water. The ZnO nanoparticles were found to be hexagonal. The size distribution of generated ZnO nanoparticles is decreased by increasing the laser pulse energy. The rate of ZnO nanoparticles production is increased with increasing the laser pulse energy and is decreased with increasing the laser photon energy. ZnO nanoparticles were formed with different shapes depending on the laser pulse energy and laser wavelength. The bandgap energy for ZnO nanoparticles generated with 1064 nm laser pulse wavelength is calculated to be 3.59–3.89 eV.

1. Introduction

Nanoparticles are of great interest for many technological applications and fundamental research due to their size-dependent physical properties [1]. One of the most versatile materials in nanotechnology is zinc oxide (ZnO), a semiconductor with a great application potential in optics, energy conversion and biomedicine [2]. ZnO, due to its numerous significant properties, such as catalytic, electrical, electronic, chemical stability, low dielectric constant, optical and effective antimicrobial, antibacterial and bactericide, has drawn increasing concentration in recent years [3]. Additional advantages of ZnO are that it can be easily processed by wet chemical etching and that it has excellent stability under high-energy radiation [4]. ZnO is an interesting chemically and thermally stable n-type semiconductor with high exciton binding energy (60 meV), wide direct bandgap of 3.37 eV at room temperature and high sensitivity to toxic and combustible gases [5,6]. ZnO is the richest family of nanostructures among all semiconducting materials, both in structures and in properties due to its unique properties [7].

A wide variety of techniques have been exploited to fabricate ZnO nanostructures. Most well-defined ZnO nanostructures with an abundant variety of shapes, such as nanorods, nanoneedles, nanotubes, nanobelts, flower-, spindle-, and tower-like structures, have been synthesized by traditional methods based on the high-temperature vapor-based techniques or the chemical solution route [5]. Among others, the pulsed laser ablation (PLA) method has

been attracting much interest for producing organic nanoparticles and is better suited for organic compounds that are non-water soluble or water soluble resistant [8]. The important features of the PLA technique are that one can prepare well crystallized nanoparticles which are pure without by-products [9]. The PLA technique for synthesis of nanostructured materials from a solid target in liquid media has many advantages. The first advantage of the PLA technique is inexpensive equipment for controlling the ablation atmosphere. Most importantly, it has been demonstrated that size of synthesized material can be controlled by changing different parameters such as laser wavelength, laser fluence, pulse laser duration, changing the pH of the solution, adding surfactants and changing the temperature of solution [10–12].

Reports on the production of ZnO nanoparticles by laser ablation can be classified in three categories. Many of them have investigated the effect of laser environment on the characteristics of ZnO nanoparticles [5,13,14]. In most of them the third harmonic of Nd-YAG laser was employed to generate ZnO nanoparticles [5,10,12], while we have used the first and second harmonics of Nd-YAG laser. And rarely the effect of laser pulse energy and wavelength in producing ZnO nanoparticles is reported [15].

In this paper for the first time the 470–1500 mJ laser pulse energy is employed to produce ZnO nanoparticles. We present experimental results on the formation of ZnO nanoparticles via laser ablation in deionized water, which clearly demonstrate the effect of laser pulse energy and wavelength on the nanostructure, morphology, and optical properties of ZnO nanoparticles at room temperature in the high laser pulse energy regime. It is shown that by changing the laser pulse energy or wavelength a new class of ZnO nanoparticles can be produced via laser ablation process.

* Corresponding author. Tel./fax: +98 21 44869654.
E-mail addresses: doran@srbiau.ac.ir, d.dorranian@gmail.com (D. Dorranian).

2. Experimental details

ZnO nanoparticles were produced by PLA of a Zn plate (99.9%) in deionized water. A zinc metal plate was placed in the bottom of an open glass cylindrical vessel filled with 25 mL of deionized water. Height of water on the target was 2 cm. The Zn plate was cleaned ultrasonically in alcohol, acetone and deionized water before the experiments. Plate was ablated with a pulsed Nd:YAG laser operated at 10 Hz repetition rate with 6 ns pulse width for 7 mins. ZnO nanoparticles were produced using the 1064 nm wavelength of Nd:YAG laser at 0.75–1.5 J energy and 532 nm wavelength of Nd:YAG laser (second harmonic) at 0.47 and 0.63 J pulse energy. The laser beams of 2 mm (532 nm) and 2.5 mm (1064 nm) in diameter were focused using a lens with a focal length of 85 mm. The spot sizes of laser pulse on the target surface were 23.03 μm, and 14.39 μm for 1064 nm and 532 nm laser wavelengths respectively. Detail about the samples preparation is presented in Table 1. ZnO nanoparticles solution turns brown just after ablation, and then changed to a colorless solution after few hours. Pictures of nanoparticle solutions are presented in Fig. 1 (a) and (b). The ablated mass was determined by weighing the substrate before and after the ablation process (using KERN 770 scale), with an accuracy of 0.1 mg.

A variety of analytical techniques were applied for the characterization of products. The crystalline structure of the samples was analyzed by X-ray diffraction (XRD) with Cu-Kα radiation ($\lambda = 1.54060$ Å), using an STOE–XRD diffractometer. The suspensions were dropped onto Si substrates and dried for XRD measurement. Also their morphology was investigated by LEO440i scanning electron microscopy (SEM). The optical properties of the nanoparticle solution were examined at room temperature by a UV–vis absorption spectrophotometer PG instruments Ltd. Particle size and size distribution were measured by a dynamic light scattering (DLS) apparatus MALVERN ZETASIZER 3000HS$_A$. Transmission electron microscopy (TEM, Philips EM 208) was done by placing a drop of the concentrated suspension on a carbon-coated copper grid.

Table 1
Laser wavelength and pulse energy of samples produced by PLA.

Laser wavelength (nm)	532		1064			
Pulse energy (J)	0.47	0.63	0.75	1	1.25	1.5
Sample number	1	2	3	4	5	6
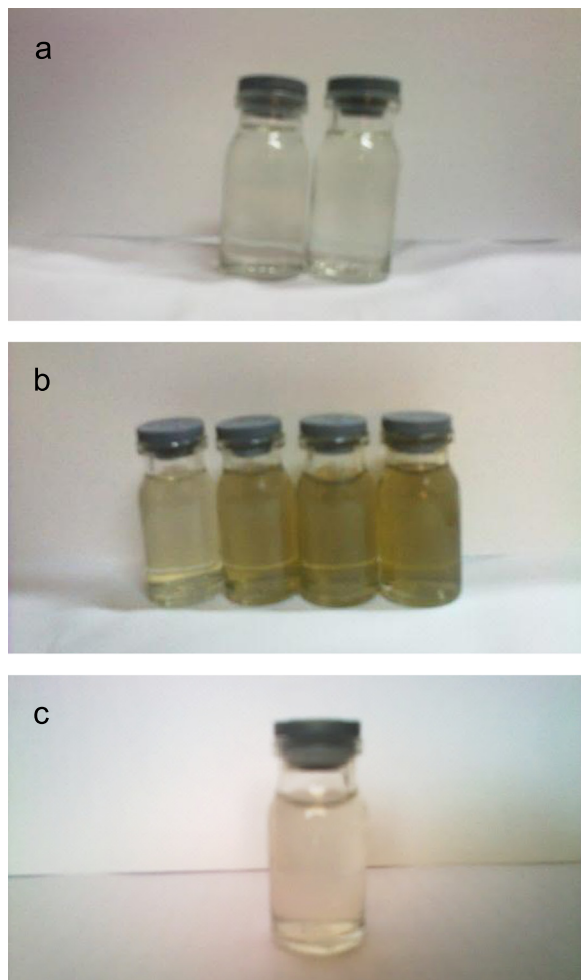
Fig. 1. ZnO nanoparticles solution generated by 532 nm laser pulse wavelength (a) and 1064 nm laser pulse wavelength (b) just after production. Few hours after production, all samples changed as is shown in (c).

3. Results and discussion

3.1. Ablation rate

Ablation rate versus laser pulse energy density is presented in Fig. 2. Unfortunately the laser system was not capable to emit laser beam at 532 nm wavelength with energy density larger than 20 J/cm². In both cases the ablation rate of Zn with 1064 nm wavelength is larger than with 532 nm wavelength. It shows that both photon energies are enough for ablating but smaller number of photons in 532 nm wavelength laser beam leads to small rate of ablation. Another result of Fig. 2 is the linear behavior of ablation rate of Zn nanoparticles with laser pulse energy density. The slope of the line is about 0.67 g cm²/J s.

Two parameters should be noticed. One is the laser pulse energy. Our results show that with increasing the laser pulse energy, the ablation rate is increased, which is a clear result and is in good agreement with other reports. Second is the laser photon energy. With increasing the photon energy, while the pulse energy is constant, the ablation rate decreases. It may be due to this reason that in this experimental condition the ablation rate depends more on the number of photons rather than photon energy.

3.2. XRD studies of ZnO nanoparticles

XRD spectrum of sample 6 is presented in Fig. 3. X-ray diffraction measurement was performed for the dried film from the concentrated suspension on a Si substrate. In Fig. 3 a peak of X-ray photons diffracted from Si substrate can be seen at $2\theta = 69.4°$.
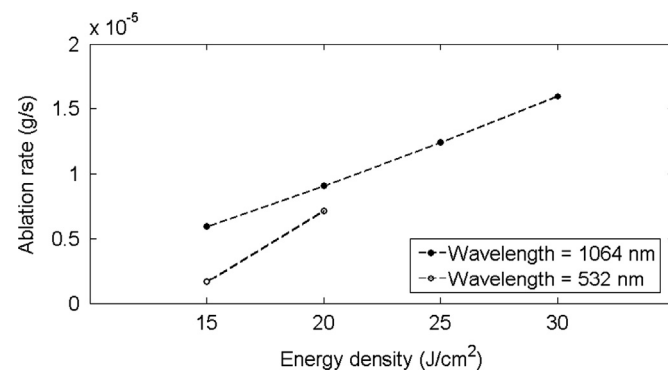
Fig. 2. Ablation rate versus laser pulse energy density.

The XRD spectrum clearly shows the crystalline structure of the nanoparticles and various peaks of zinc oxide (ZnO). On the other hand, the sample prepared in pure water exhibits diffraction peaks from ZnO nanoparticle [16]. The main dominant peaks of ZnO were identified at $2\theta = 31.8°$, $34.5°$, $36.3°$, $47.6°$, $56.7°$, and $63.1°$. There was no peak in the spectrum of samples 1–2 which were prepared by the 532 nm laser pulse wavelength. It may be due to small number of nanoparticles in crystalline structure. The XRD pattern of the ZnO nanoparticles formed by 1064 nm wavelength laser beam in deionized water at room temperature reveals that they are crystalline and possess the hexagonal wurtzite structure. We have obtained polycrystalline of nanoparticles when their intensity of peaks is changed randomly for different samples. It can be concluded that Zn and O atoms are composed randomly during the ablation process.

The average grain size 'd' of the nanoparticle of ZnO generated by laser ablation was estimated by using the standard Eq. (1) known as the Scherrer formula [17]

$$d = \frac{k\lambda}{\beta \cos \theta} \tag{1}$$

where k = constant $(0.89 < k < 1)$, λ = wavelength of the X-ray, β = Full Width at Half Maximum (FWHM) of the diffraction peak, and θ = diffraction angle. The mean grain size of (002) oriented ZnO calculated using the above mentioned Eq. (1), which is listed
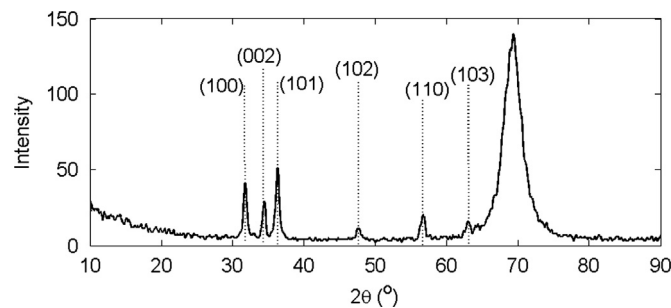
in Table 2. The grain size of nanoparticles generated with 1064 nm wavelength was decreased by increasing the laser pulse energy. Decreasing the grain size with increasing the laser pulse energy is in good agreement with the recently reported work by Fazio et al. [15].

With increasing the laser pulse energy, adhesion of nanoparticles decreases leads to decrease the grain size of samples. This can be observed in the SEM micrographs. Calculated grain size of other plains varies randomly in the range of 13–40 nm.

There are two lattice constants for hexagonal unit cell, known as 'a' and 'c' which can be calculated from XRD spectrum of samples by the following equation [18]:

$$\frac{1}{d^2} = \frac{4}{3}\left(\frac{h^2 + k^2 + hk}{a^2}\right) + \frac{l^2}{c^2} \tag{2}$$

where h, k, and l, are known as the Miller indices. Lattice constant of unit cell of samples 4–6 is presented in Table 2. Magnitudes of lattice constants a and c are comparable with Ref. [9].

3.3. Size of nanoparticles

Size distribution of samples has been measured using the DLS method. That is one of the most reliable methods to measure the size distribution of nanoparticles. The plots of size distribution of samples are presented in Fig. 4. We did not have any result from nanoparticles generated with 532 nm wavelength of laser pulse. Again this can be due to small number of nanoparticles in deionized water. Smaller ablation rate clearly confirms that in the case of samples which were produced by 532 nm laser pulse, number of particles is small [19]. According to skin depth magnitude $\delta = (2/\mu\sigma\omega)^{1/2}$, in which μ is the target permittivity, σ is the target conductivity and ω is the electromagnetic field angular frequency, the penetration depth of 532 nm laser pulses in target is half of this length for 1064 nm laser pulse. In this case for 532 nm laser pulse the number of ablated particles is small. Nanoparticles generated with 1064 nm wavelength of laser pulse are between 30 and 120 nm, but as is clear in Fig. 4 their size decreased with increasing the laser pulse energy. Increasing the energy of laser pulse leads to increasing the kinetic energy of ablated particles in the plasma plume generated on the surface of target during ablation. In other words we have particles at higher temperature and probability of adhesion of particles is decreased so smaller particles will be generated. According to DLS results the size distribution of generated nanoparticles is also decreased by increasing the laser pulse energy. We have more uniform nanoparticles at higher laser pulse energy.

Fig. 3. X-ray diffraction of ZnO nanoparticles prepared by pulsed laser ablation in deionized water.

Table 2
Lattice parameters and grain size at different samples.

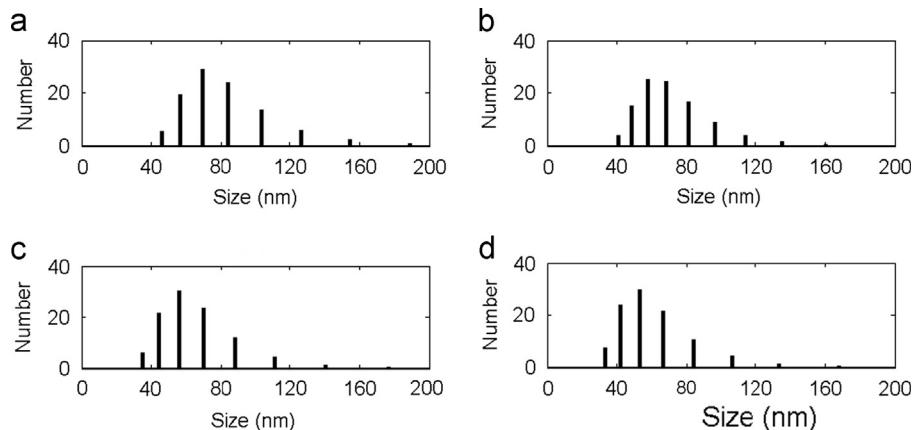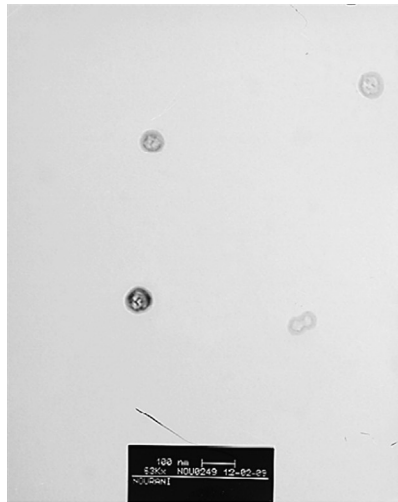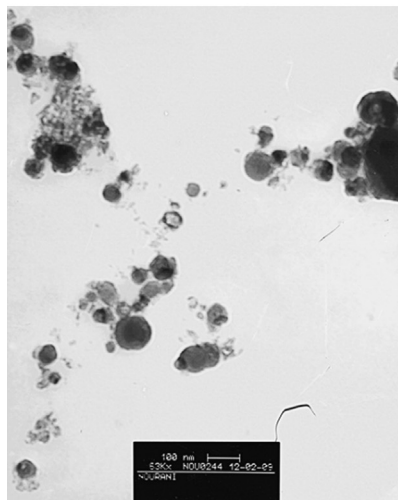| Sample	θ_{100}	a (Å)	θ_{002}	c (Å)	Grain size (nm)
4	31.750	3.2543	34.360	5.3399	22.41
5	31.824	3.2469	34.529	5.1952	17.60
6	31.859	3.2435	34.356	5.2206	16.54

Fig. 4. Plots of size distribution (a) sample 3, (b) sample 4, (c) sample 5, and (d) sample 6, measured by the DLS method.
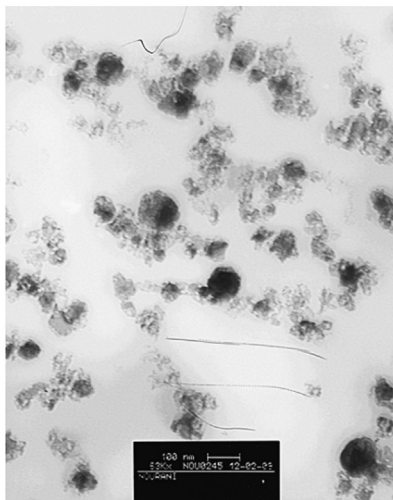
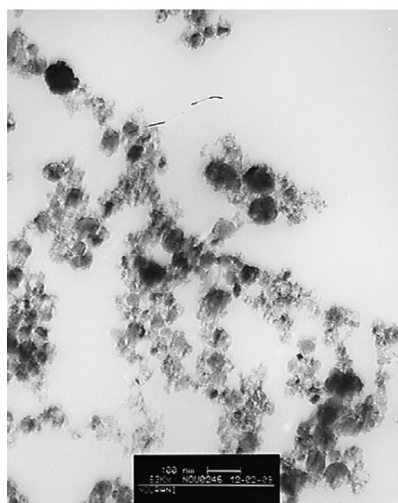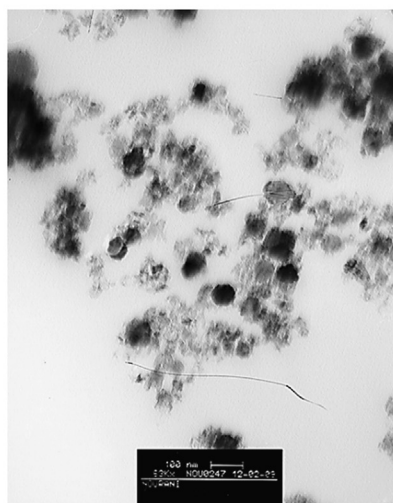Sample 1   Sample 2

Sample 3   Sample 4

Sample 5   Sample 6

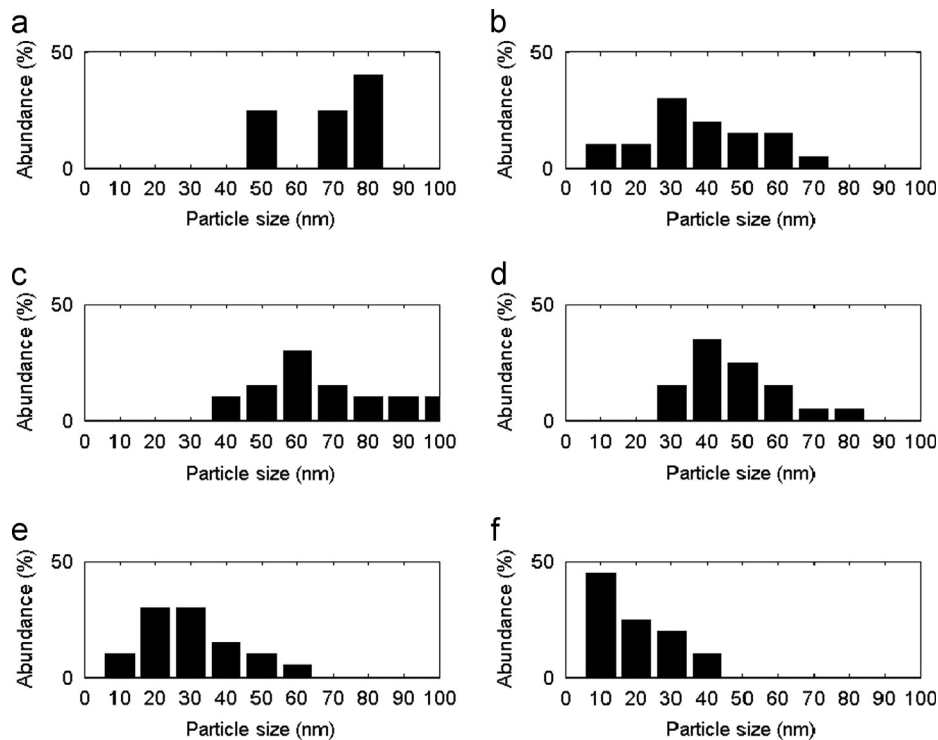**Fig. 5.** TEM micrographs of ZnO nanoparticles.

Fig. 6. Size distribution of (a) sample 1, (b) sample 2, (c) sample 3, (d) sample 4, (e) sample 5, and (f) sample 6, extracted from TEM images.

TEM images of the nanoparticles on the scale of 100 nm are displayed in Fig. 5. As can be seen, the ZnO nanoparticles are almost spherical in all samples [16] and the particle sizes and size distribution are related to the laser pulse energy and laser wavelength. In Fig. 6, the size distribution graphs of ZnO nanoparticles are shown. It can be seen that with increasing the laser pulse energy, sizes of nanoparticles are decreased. Similar results can be observed in DLS measurement. Measured size of nanoparticles with the DLS method is larger than those which is obtained in TEM micrographs. DLS measurement determines the hydrodynamic sizes of the synthesized nanoparticles which are significantly larger than their real size which is indicated in TEM images.

The same results have been reported by Fazio et al. [15]. They produced ZnO nanoparticles in water by laser ablation process using 532 nm laser wavelength at 20–50 mJ pulse energy. Recently, Kim et al. have presented a work on the effect of laser wavelength (1064, 532, and 355 nm), and fluence (50–130 mJ/pulse) on the characteristics of ZnO nanoparticles produced by the laser ablation method. They reported that, the size and shape of nanoparticles were affected slightly only by the fluence of 1064 nm wavelength pulse, and the nanoparticles formed by ablation at 355 nm had a distinctive wire-shape with a small diameter [20].

3.4. Morphology of nanoparticles

Fig. 7 shows the SEM images of ZnO nanoparticles prepared by laser ablation in deionized water. Morphology of ZnO nanoparticles depends on laser pulse energy and also is influenced by laser pulse wavelength. As can be seen, the density of ZnO nanoparticles in water increased with increasing the fluency of laser beam. Shape of nanoparticles which are produced by laser ablation of a solid target in liquids may be a combination of different shapes. In this case we classify the shape of samples upon their predominant shape of nanoparticles. The particles prepared by laser pulse of 532 nm wavelength were spherical and adhered to each other. This

structure is similar to those reported in Ref. [10] prepared at room temperature. Particles prepared by laser pulse of 1064 nm wavelength are sheet-like and spherical nanostructures. The size and amount of sheet-like nanostructures decreased by increasing the laser pulse energy. On the other hand with increasing the laser pulse energy the amount of the spherical nanostructures in the solution increased. So the morphology of nanoparticles strongly depends on the energy and wavelength of laser pulse in the experiment. Again in this result the effect of higher energy particles can be observed. With increasing the laser pulse energy, adhesion of particles decreases leads to decrease the size of sheet-like structures.

These different morphologies strongly depends on the characteristics of generated plasma on the surface of target according to interaction of high power laser pulse with solid target. In fact, hydrosols are always electrolytes containing various positively and negatively charged ions. Bringing a metal electrode with excess charge into this electrolyte, this excess charge will be screened by the ions in the electrolyte. This is achieved by a thin ion layer in direct contact to the electrode – the Stern layer – followed by a diffuse ion cloud extending in the electrolyte. Both form the so-called double layer. The extension of the cloud is given by the Debye–Hückel screening length $1/\kappa$ with the Debye–Hückel parameter given by [21]

$$\kappa = \frac{e^2}{\varepsilon\varepsilon_0 k_B T} \sum_j n_j z_j^2 \qquad (3)$$

where n_j is the concentration and z_j is the ion valence of ions of kind j and k_B is the Boltzmann constant. T is the temperature which is increased by increasing the laser pulse energy. With decreasing κ the repulsive Coulomb potential will be increased while the attractive van der Waals potential between particles will be decreased. So on increasing the laser pulse energy aggregation
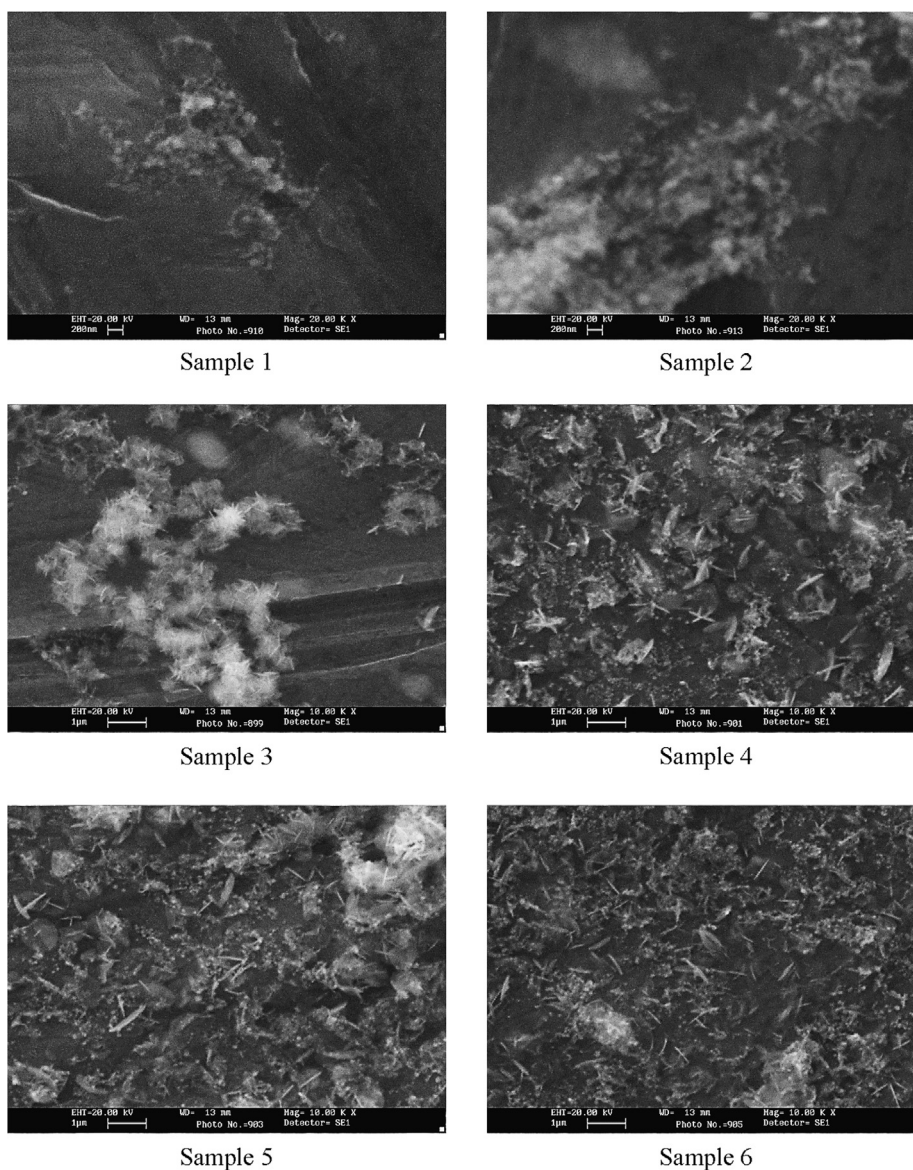
Fig. 7. SEM images of ZnO nanoparticles prepared by pulsed laser ablation in deionized water.

will be decreased. In these cases the number of spherical particles in the solution will be increased [21].

3.5. UV absorption spectrum of ZnO

The optical absorbance of suspended ZnO nanoparticles prepared by PLA in water was measured in the 200–1100 nm wavelength range with respect to deionized water absorption as the base line. Fig. 8 presents optical absorption spectra of ZnO nanoparticle solutions. It exhibits UV absorption peak from the exciton absorption of ZnO nanoparticles at 292–323 nm. The intensity of absorption peak is increased sharply from sample 3 to samples 4–6. It can be due to the higher number of particles in samples 4–6 in comparison with sample 3. According to Ref. [14], decreasing the width and increasing the intensity of absorption peak of these samples can also be attributed to decreasing the aggregation of particles [14]. When the size of semiconductor nanoparticles, is comparable to or below their exciton Bohr radius, they have distinctive electronic and optical behaviors due to
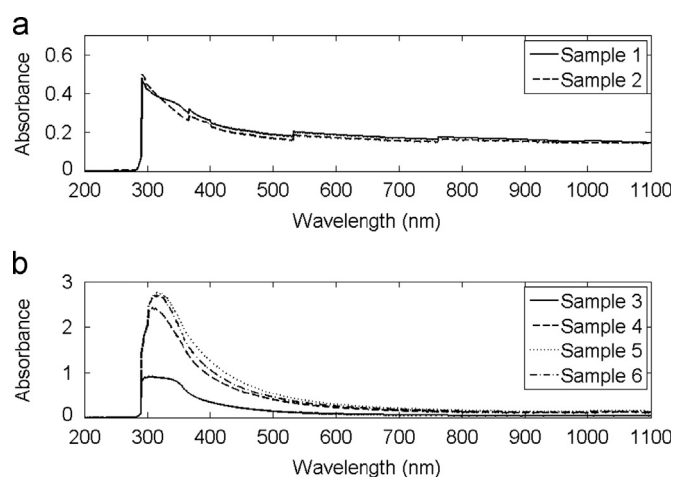

Fig. 8. Absorption spectra of ZnO nanoparticles in deionized water prepared at (a) 532 wavelength and (b) 1046 wavelength.
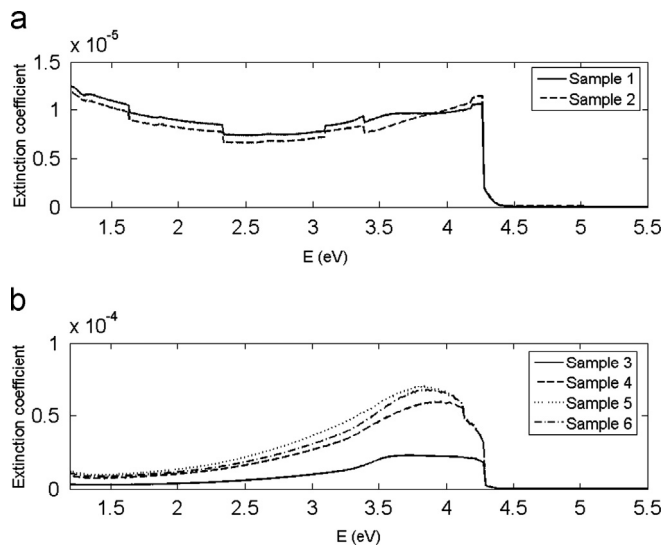
a

b

Fig. 9. Extinction coefficient spectra of ZnO nanoparticles in deionized water prepared at (a) 532 wavelength and (b) 1046 wavelength.

exciton quantum confinement phenomena [9]. It is clear that the absorption edge systematically shifts to the lower wavelength with decreasing size of the nanoparticle. This pronounced and systematic shift in the absorption edge is due to the quantum size effect. The blue shift of absorption peak due to quantum confinement effect can be observed in the spectra. Nanoparticles generated by 532 nm laser wavelength are smaller so larger blue shift occurred for their absorption peak. In the quantum confinement range, the bandgap of the particle increases resulting in the shift of absorption edge to lower wavelength, as the particle size decreases.

The extinction coefficient of sample $k = \alpha\lambda/4\pi$ is plotted versus photon energy in Fig. 9. In this relation α is the absorption coefficient and λ is the wavelength. The spectrum of extinction coefficient of nanoparticles generated with 532 nm wavelength of laser pulse has a maximum at about 4.3 eV while for nanoparticles generated with 1064 nm wavelength of laser pulse this maximum appeared at 3.9 eV photon energy. It can be explained that the peak of extinction coefficient is due to a resonant absorption in the ZnO nanoparticles.

The parabolic dependence of absorption coefficient on photon energy is commonly used to determine the bandgap of the semiconductor nanoparticles and involves extrapolating $(\alpha h\upsilon)^2$ versus photon energy $(h\upsilon)$ to $\alpha = 0$. This approach not only underestimates the bandgap but also fails to account for the large excitonic effect in GaN and ZnO. A more accurate way to determine the bandgap is to determine the change in curvature or the energy at which the slope or derivative of the absorption spectrum is maximum. This corresponds to a positive curvature below the bandgap and a negative curvature above the bandgap and onset of band-to-band transition when the curvature changes in the

absorption spectrum [22]. Using this method the bandgap energy for nanoparticles generated with 1064 nm laser pulse wavelength is found to be 3.59–3.89 eV. But for nanoparticles generated with 532 nm laser pulse wavelength the absorption edge is not clear and this method cannot be used for calculating their bandgap energy. Size of nanoparticles in samples 1 and 2 is smaller than their size in samples 3–6. The extracted bandgap energy of our samples is in good agreement with other reported magnitudes [16,23,24].

4. Conclusion

ZnO nanoparticles were synthesized by pulse laser ablation in deionized water without using any surfactant. In this work, the effects of laser pulse energy and laser wavelength on the nanostructure, morphology, optical properties of ZnO nanoparticles have been investigated.

XRD data reveal that these nanoparticles possessed the hexagonal wurtzite structure. The size distribution of ZnO nanoparticles decreased with increasing the laser pulse energy that can be attributed to decreasing the aggregation of particles. Two forms of sheet-like and spherical nanostructures were observed due to variation of laser pulse energy and wavelength. The blue shift in the absorption edge indicates the quantum confinement property of nanoparticles.

References

[1] Noel S, Hermann J, Itina T. Appl Surf Sci 2007;253:6310–5.
[2] Wagener Ph, Faramarzi Sh, Schwenke A, Rosenfeld R, Barcikowski S. Appl Surf Sci 2011;257:7231–7.
[3] Abdolmaleki A, Mallakpourb Sh, Borandeh S. Appl Surf Sci 2011;257:6725–33.
[4] Djurisic AB, Ng AMC, Chen XY. Prog Quantum Electron 2010;34:191–259.
[5] He Ch, Sasaki T, Shimizu Y, Koshizaki N. Appl Surf Sci 2008;254:2196–202.
[6] Patil LA, Bari AR, Shinde MD, Deo V. Sens Actuators B 2010;149:79–86.
[7] Mote VD, Purushotham Y, Dole BN. J Theor Appl Phys 2012;6:6.
[8] Li B, Kawakami T, Hiramatsu M. Appl Surf Sci 2003;210:171–6.
[9] Gondal MA, Drmosh QA, Yamani ZH, Saleh TA. Appl Surf Sci 2009;256:298–304.
[10] Ishikawa Y, Shimizu Y, Sasaki T, Koshizaki N. J Coll Interface Sci 2006;300:612–615.
[11] Solati E, Mashayekh M, Dorranian D. Appl Phys A 2013;112:689–94.
[12] Drmosh QA, Gondal MA, Yamani ZH, Saleh TA. Appl Surf Sci 2010;256:4661–6.
[13] Zamiri R, Zakaria A, Abbastabar Ahangar H, Darroudi M, Khorsand Zak A, Drummen GPC. J Alloys Compd 2012;516:41–8.
[14] He Ch, Sasaki T, Usui H, Shimizu Y, Koshizaki N. J Photochem Photobiol A 2007;191:66–73.
[15] Fazio E, Mezzasalma AM, Mondio G, Neri F, Saija R. Appl Surf Sci 2013;272:30–35.
[16] Zeng H, Cai W, Li Y, Hu J, Liu P. J Phys Chem B 2005;109:18260–6.
[17] Suryanarayana C, Norton MG. X-ray diffraction a practical approach. New York: Plenum Press; 1998.
[18] Tiemann M, Marlow F, Hartikainen J, Weiss O, Linder M. J Phys Chem C 2008;112:1463–7.
[19] Dorranian D, Solati E, Dejam L. Appl Phys A 2012;109:307–14.
[20] Kim KK, Kim D, Kim SK, Park SM, Song JK. Chem Phys Lett 2011;511:116–20.
[21] Quinten M. Optical properties of nanoparticle systems. Boschstr. 12, 69469 Weinheim, Germany: Wiley-VCH Verlag & Co. KGaA; 2011.
[22] Bajaj G, Soni RK. Appl Surf Sci 2010;256:6399–402.
[23] Ajimsha RS, Anoop G, Aravind A, Jayaraj MK. Electrochem Solid-State Lett 2008;11:K14–7.
[24] Cho JM, Song JK, Park SM. Bull Korean Chem Soc 2009;30:1616–8.